Check for updates

A Low-Cost and Recyclable Mg/SOCl₂ Primary Battery Via Synergistic Solvation and Kinetics Regulation

Qiuchen Xu, Shitao Geng, Bin Yuan, Meng Liao, Lei Ye, Xiaoju Zhao, Yan Wang, Xiao Zhang, Shuo Wang, Zongtao Qu, Han Miao, Zhibin Yang, Yue Gao, Bingjie Wang, Yongfeng Zhou, Huisheng Peng, and Hao Sun*

Lithium/thionyl chloride (Li/SOCl₂) primary batteries are appealing power solutions because of their remarkable electrochemical performances. However, their mass applications are hindered by the challenges in sustainability, cost and safety concerns owing to the employed Li chemistry. Here, magnesium (Mg) chemistry is shown as a promising alternative through synergistic optimization of electrolyte solvation and electrode reaction kinetics. The first Mg/SOCl₂ primary battery yields surprisingly high specific capacities up to ≈14 000 mAh g⁻¹ at a decent discharge voltage of ≈1.67 V, which outperforms the state-of-the-art Mg-based primary batteries. In addition, it retains almost 100% of the original capacity after 20-day reservation. The impressive battery performances are originated from the stabilized MgCl₂ formation on high-surface-area carbon cathode and suppressed Mg anode corrosion via the Mg-induced solvation effect. Mg/SOCl₂ primary batteries are promising candidates for low-cost and recyclable power supplies, and they thus open new avenues for the development of sustainable battery chemistries.

1. Introduction

Electrochemical energy storage devices are key building blocks of modern electronics.[1] Among them, lithium/thionyl chloride (Li/SOCl₂) primary battery represents an important branch with a global market exceeding US$ 2 billion per year, which has been actively pursued since its invention in the 1970s.[2] It employs the catholyte comprised of SOCl₂ and metal chlorides to perform the redox reaction between metallic lithium and

SOCl₂,[3] affording remarkable specific capacities of over 2000 mAh g⁻¹ and a high energy density of ≈590 Wh kg⁻¹ in a single discharge.[4] Over the past half a century, considerable efforts have been made to improve the discharge capacity and rate capability of Li/SOCl₂ primary battery,[5] making it an indispensable candidate in a broad range of practical applications including industrial instruments, pacemakers, and aerospace facilities.[3a,6]

Despite of the above advantages, it remains challenging to make Li/SOCl₂ primary batteries sustainable owing to the employment of Li chemistry. For instance, the low earth abundance (0.0017%) of Li element has greatly hindered the sustainability of Li/SOCl₂ battery, as evidenced by the rapidly rising prices of Li-based raw materials in recent years.[7] Moreover, the use of highly active Li metal inevitably raises safety concerns with cost and recycling issues in large-scale applications.[8] Therefore, it is important to extend the Li-based chemistry to other metal chemistries toward promoted sustainability, safety, and recyclability.[9] However, it remains challenging to perform controllable electrochemical reactions to the best of our knowledge, owing to the challenges in synergistic regulation on the solvation effect and reaction kinetics in highly active SOCl₂-based electrolytes.

Herein, the first magnesium/thionyl chloride (Mg/SOCl₂) primary battery was developed based on synergistic solvation and kinetics regulation. Commercially available ketjenblack (KJ) carbon black and Mg metal foil are employed as the cathode and anode, respectively, coupling with a low-cost SOCl₂-based catholyte with rational solvation regulation. The Mg/SOCl₂ primary battery delivers remarkable specific capacities up to ≈14 000 mAh g⁻¹ (based on the KJ mass) with a flat discharge plateau at ≈1.67 V, and affords decent rate capability at 50 to 2000 mA g⁻¹. Additionally, it shows no capacity or voltage loss after a 20-day reservation. We show the key factors that determine battery performances, i.e., stabilized MgCl₂ formation and suppressed Mg anode corrosion via synergistic promotion of reaction kinetics and Mg-induced solvation effect. The electrodes from a "dead" Mg/SOCl₂ primary battery can be readily recycled through a simple and efficient process, recovering 89% and 99% of the initial capacity and discharge voltage, respectively. As a proof-of-concept, our Mg/SOCl₂ primary

Q. Xu, S. Geng, B. Yuan, X. Zhao, Y. Wang, X. Zhang, S. Wang,
Z. Qu, H. Miao, Z. Yang, Y. Zhou, H. Sun
Frontiers Science Center for Transformative Molecules
School of Chemistry and Chemical Engineering, and Zhangjiang
Institute for Advanced Study
Shanghai Jiao Tong University
Shanghai 200240, China
E-mail: haosun@sjtu.edu.cn
M. Liao, L. Ye, Y. Gao, B. Wang, H. Peng
State Key Laboratory of Molecular Engineering of Polymers
Department of Macromolecular Science, and Laboratory
of Advanced Materials
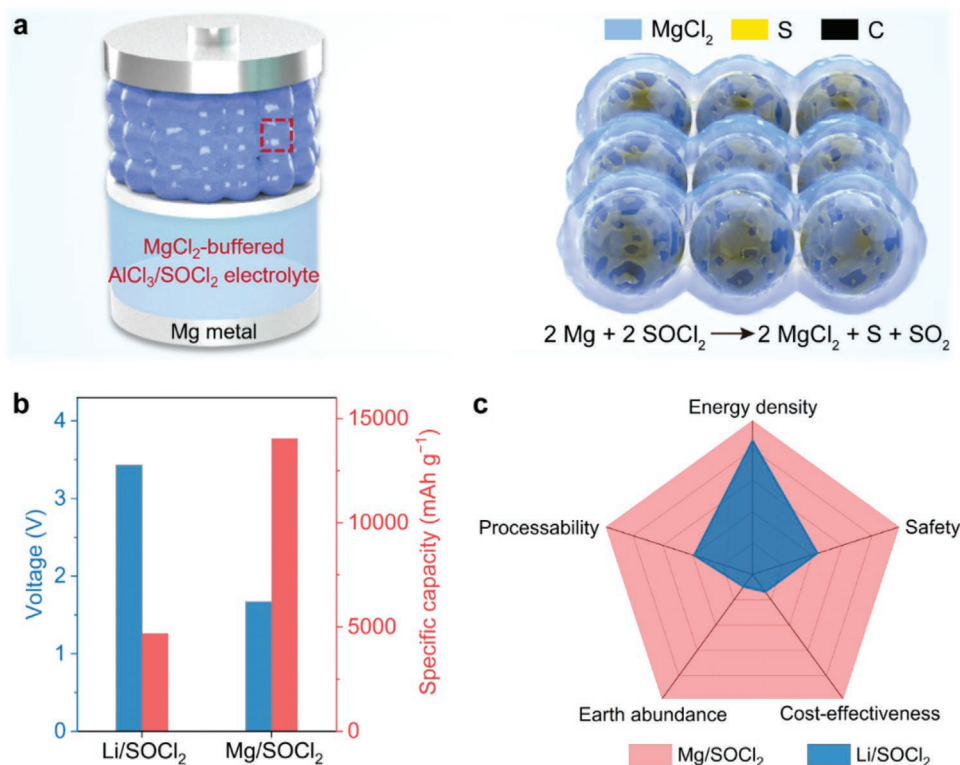Fudan University
Shanghai 200438, China

Figure 1. Configuration and characteristics of our Mg/SOCl₂ primary battery. a) Schematic illustration of a Mg/SOCl₂ primary battery comprised of a KJ loaded Ni foam cathode, a Mg foil anode and an optimized catholyte comprised of 2 M AlCl₃ and 0.8 M MgCl₂ dissolved in SOCl₂. The scheme on the right shows the main discharge products including MgCl₂ and S-based species on carbon cathode. b) Comparison on the main discharge parameters including voltage and specific capacity of Li and Mg/SOCl₂ primary batteries. c) Comparison on the earth abundance, energy density, safety, cost-effectiveness, and processability of Li and Mg/SOCl₂ primary batteries. More details on the cost-effectiveness and processability are provided in Tables S1 and S2 (Supporting Information).

batteries can serve as sustainable power supplies in a variety of practical applications with high safety, low cost, and high recyclability.

2. Results and Discussion

In our attempt to produce Mg/SOCl₂ primary battery, we used a Mg metal foil as the anode and conductive carbon black loading on nickel (Ni) foam as the cathode in coin cells (**Figure 1**a). Our electrolyte (catholyte) is 2 M AlCl₃ and 0.8 M MgCl₂ dissolved in SOCl₂. The battery experiences a primary discharge through Mg anode oxidation into Mg²⁺ and SOCl₂ catholyte reduction into S, SO₂, and Cl⁻. The discharge reaction can be described as follows:

$$2Mg(s) + 2SOCl_2(l) \rightarrow 2MgCl_2(s) + S(s) + SO_2(g) \quad (1)$$
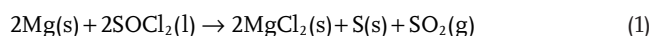
Compared with Li/SOCl₂ primary batteries, our Mg/SOCl₂ primary batteries showed much higher specific capacities of over 14000 mAh g⁻¹ with a discharge voltage of 1.67 V at 50 mA g⁻¹ based on the mass of carbon under the same condition (Figure 1b; Figure S1, Supporting Information). Additionally, our Mg/SOCl₂ primary batteries showed significant advantages in earth abundance, safety, cost-effectiveness, and processability, as well as comparable energy densities

over the Li/SOCl₂ counterpart owing to the Mg-based materials and chemistry (Figure 1c; Tables S1 and S2, Supporting Information).

The battery performances were highly dependent on the electrolyte composition. For instance, the battery using electrolyte comprised of high-concentration (4 M) AlCl₃ in SOCl₂ (named HC-A-SOCl₂) delivered both low discharge voltage (≈0.2 V) and specific capacity (2461 mAh g⁻¹) at 100 mA g⁻¹ (**Figure 2**a), because the reduction of Al₂Cl₇⁻ anions derived from high-concentration AlCl₃ that formed metallic Al deposition on Mg anode hindered normal battery discharge.[10] By contrast, the battery based on a relatively dilute electrolyte of 2 M AlCl₃ in SOCl₂ (named A-SOCl₂) demonstrated a much higher discharge plateau (1.59 V) and specific capacity (8258 mAh g⁻¹). Further, a dramatically increased specific capacity of over 11000 mAh g⁻¹ was achieved through the addition of 0.8 M MgCl₂ salt into the A-SOCl₂ electrolyte (named A-M-SOCl₂). This could be attributed to the suppressed discharge product (MgCl₂) dissolution into A-M-SOCl₂ electrolyte with the existence of 0.8 M MgCl₂, which stabilized the discharge product on the cathode during discharge. The presence of Mg-based cations (e.g., MgCl⁺ and Mg²⁺) in the electrolyte could also facilitate MgCl₂ formation kinetics on cathode owing to their strong interactions with AlCl₄⁻ anions,[11] as evidenced by the increased discharge voltage using A-M-SOCl₂ electrolyte.
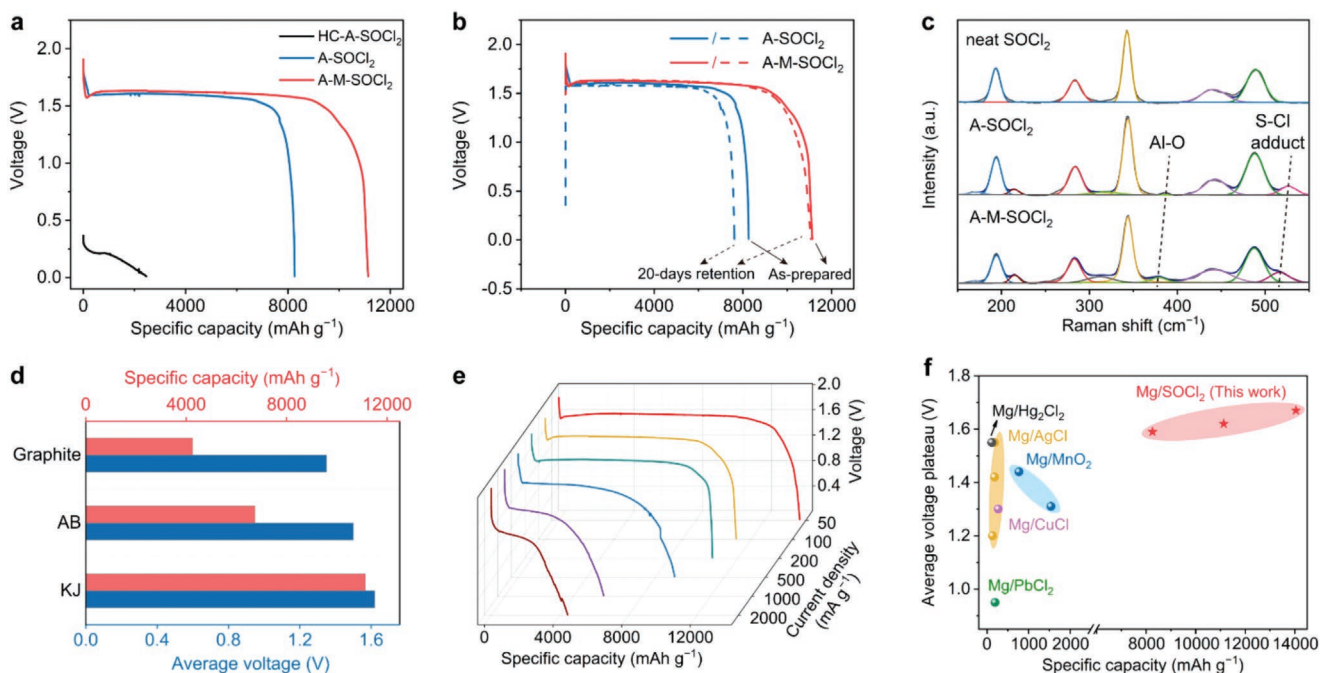
ADVANCED
SCIENCE NEWS
www.advancedsciencenews.com

ADVANCED
FUNCTIONAL
MATERIALS
www.afm-journal.de

Figure 2. Electrochemical performances of our Mg/SOCl$_2$ primary batteries. a) Galvanostatic discharge curves of Mg/SOCl$_2$ primary batteries using HC-A-SOCl$_2$, A-SOCl$_2$, and A-M-SOCl$_2$ electrolytes at the same current density of 100 mA g^{-1}. b) Galvanostatic discharge curves of Mg/SOCl$_2$ primary batteries using A-SOCl$_2$ and A-M-SOCl$_2$ electrolytes with and without 20-day retention. The solid and dotted lines represent the curves of as-prepared and 20-day-retention batteries, respectively. c) Raman spectra of neat SOCl$_2$, A-SOCl$_2$, and A-M-SOCl$_2$ electrolytes. d) Comparison on the electrochemical performances of Mg/SOCl$_2$ primary batteries using KJ, AB, and graphite as the cathodes. e) Galvanostatic discharge curves of Mg/SOCl$_2$ primary batteries at increasing discharge current densities from 50 to 2000 mA g^{-1}. f) Comparison on the performances of our Mg/SOCl$_2$ primary batteries with other Mg-based primary batteries, e.g., Mg/MnO$_2$,[14] Mg/AgCl,[15] Mg/CuCl,[15c] Mg/PbCl$_2$[15c], and Mg/Hg$_2$Cl$_2$.[15c]

We also discovered the presence of MgCl$_2$ salt in the electrolyte could benefit the retention capability of the obtained batteries. For instance, after 20-days retention, no significant changes were observed in both discharge voltage and specific capacity using A-M-SOCl$_2$ electrolyte (Figure 2b). In contrast, the MgCl$_2$-free A-SOCl$_2$ electrolyte only retained 92.2% of the original capacity, as well as significant voltage delay at the initial discharging stage, indicating more severe polarization caused by the passivation of Mg metal anode during retention. Dissolution experiment further confirmed the importance of electrolyte composition on retention performance (Figure S2, Supporting Information). The Mg metal anode was completely dissolved in HC-A-SOCl$_2$ electrolyte overnight, and the dissolution rate was ≈0.2 mg h^{-1} in A-SOCl$_2$ electrolyte. In comparison, the Mg anode immersed in A-M-SOCl$_2$ electrolyte showed no significant mass loss overnight. Therefore, the relatively low AlCl$_3$ concentration, recognized as less corrosive to alkali metals,[12] is crucial to suppress the displacement of Al metal on Mg anode. In addition, Mg-based cations induce strong solvation with SOCl$_2$ molecules in the electrolyte, which effectively reduces the reactivity of SOCl$_2$ and Mg metal corrosion. In Raman spectroscopy, for instance, the addition of MgCl$_2$ shifted the Al-O stretching vibration to a lower frequency from 385 to 378 cm^{-1}, indicating the weakened Cl$_2$SO → AlCl$_3$ coordination induced by Mg cations (Figure 2c).[13] This is also confirmed by the shift of S-Cl symmetric stretching vibration toward lower frequency, suggesting the strengthened coordination between Mg cation and SOCl$_2$. Therefore, the Mg-based solvation

effectively reduced the reactivity of SOCl$_2$, thus suppressed the corrosion of Mg metal. The synergistic effect is critical for battery performance improvement, which represents a crucial step toward practical applications.

The detailed electrolyte screening was further performed (Figures S3 and S4, Supporting Information). For instance, electrolytes comprised of 1, 2, and 3 M AlCl$_3$ with the addition of excess MgCl$_2$ (0.4, 0.8, and 1.2 M, respectively) for saturation. Lower concentration of AlCl$_3$ (1 M) resulted in inferior battery performances, e.g., a lower specific capacity and discharge voltage of 4193 mAh g^{-1} and 1.5 V, respectively. With a higher concentration of AlCl$_3$ (3 M), the discharge voltage increased to 1.58 V, but the specific capacity of 7962 mAh g^{-1} was lower than 11 131 mAh g^{-1} of the 2 M AlCl$_3$, indicating the importance of the optimized AlCl$_3$ concentration with a comprehensively high ionic conductivity and suppressed discharge product dissolution. In addition, when the MgCl$_2$ concentration increased from 0.4 M to 0.8 M with the same AlCl$_3$ concentration (2 M), the discharge-specific capacity increased from 8398 to 11131 mAh g^{-1} at 100 mA g^{-1}, suggesting that sufficient Mg cations are important for the pursuit of high specific capacities and flat discharge plateaus. Therefore, the A-M-SOCl$_2$ electrolyte with an optimal AlCl$_3$ and MgCl$_2$ concentration of 2 M and 0.8 M was mainly used in this work.

The electrochemical performances of the Mg/SOCl$_2$ primary batteries were further optimized via carbon cathode optimization. Three carbon materials, i.e., ketjenblack (KJ), acetylene black (AB), and graphite are chosen because they

are commercially available. At similar mass loadings of 1–2 mg cm⁻², the KJ carbon was found to outperform the other groups in both specific discharge capacity (11131 mAh g⁻¹ vs 6737 and 4252 mAh g⁻¹ of AB and graphite) and voltage (1.62 V vs 1.50 and 1.35 V of AB and graphite, Figure 2d). The nitrogen absorption–desorption isotherms of different carbon materials using the Brunauer-Emmett-Teller (BET) method suggested that the specific discharge capacity was improved with the increasing specific surface area and pore volume (Figure S5 and Table S3, Supporting Information). The large specific surface area (1497.28 m² g⁻¹) and pore volume (2.96 cm³ g⁻¹) of KJ provide abundant active sites to accommodate the deposition of discharge products, which together contribute to superior battery performances.

The Mg/SOCl₂ primary battery showed decent rate capability at various discharge current densities. For instance, at 50 mA g⁻¹, the battery was capable to deliver a remarkable specific discharge capacity of 14046 mAh g⁻¹ (15.6 mAh cm⁻²) with an average discharge voltage of ≈1.67 V (Figure 2e). Even at 2000 mA g⁻¹, it could deliver a specific discharge capacity of 4465 mAh g⁻¹. The rate performance of the Mg/SOCl₂ primary battery was further evaluated at a variety of discharge current densities from 50 to 2000 mA g⁻¹ (Figure S6a, Supporting Information), suggesting excellent discharge capability at a broad range of discharge current densities. Moreover, the Mg/SOCl₂ primary battery showed promoted rate capability (10000 mA g⁻¹, 11.7 mA cm⁻²) at 50 °C (Figure S6b, Supporting Information).

Electrochemical impedance spectroscopy (EIS) results showed continuously increased electrochemical impedances of the battery during the discharge process (Figure S7, Supporting Information), corresponding to the continuous growth of MgCl₂ on the carbon cathode. With a KJ mass loading of 2–3 mg cm⁻², the Mg/SOCl₂ primary battery could deliver a decent specific capacity (8907 mAh g⁻¹) and discharge voltage (1.68 V) at 50 mA g⁻¹ (Figure S8, Supporting Information). Our Mg/SOCl₂ primary batteries showed advantageous discharge voltages (over 1.6 V vs 0.95–1.55 V) and much higher specific capacities (one to two orders of magnitude higher) compared with state-of-the-art Mg primary batteries, e.g., Mg/MnO₂,[14] Mg/AgCl,[15] Mg/CuCl,[15c] Mg/PbCl₂[15c] and Mg/Hg₂Cl₂ (Figure 2f and Table S4, Supporting Information).[15c]

Understanding the working mechanism has important implications for Mg/SOCl₂ primary batteries. We first investigated the morphology evolution of the carbon cathode upon varying the discharge depths at 100 mA g⁻¹. Pristine KJ is 50-nm nanoparticles with abundant nucleation cites that could accommodate the deposition of MgCl₂ (**Figure 3**a; Figure S9a,b). At the initial discharge state, the discharge products were first deposited on the KJ nanoparticles, and they gradually spread over the entire surface of the carbon cathode (Figure 3b–d; Figure S10, Supporting Information). As the main discharge product, the generation of MgCl₂ was confirmed by transmission electron microscopy (TEM), revealed by the cuboid crystals as well as the signature lattice fringes with a *d*-spacing of 0.593 nm
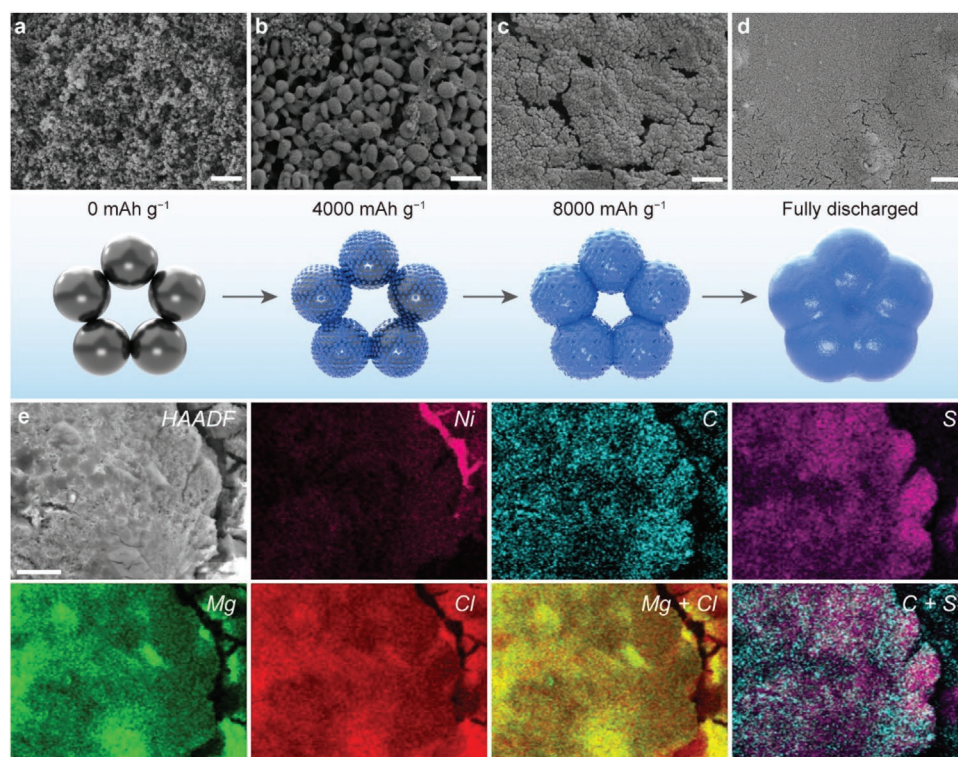

Figure 3. Cathode reaction of Mg/SOCl₂ primary batteries involves hybrid MgCl₂/S chemistry. a–d) SEM images and the corresponding schematic illustration of the discharge products on the KJ cathode at increasing discharge depths. The discharge current density is 100 mA g⁻¹. The discharge products were first deposited on the KJ nanoparticles and gradually covered the entire surface of the carbon cathode. Scale bars in a–d, 500 nm. e) Energy dispersive X-ray spectroscopy (EDS) mapping images of the fully discharged cathode show the presence of MgCl₂ and S-based species. Scale bar in e, 10 μm.
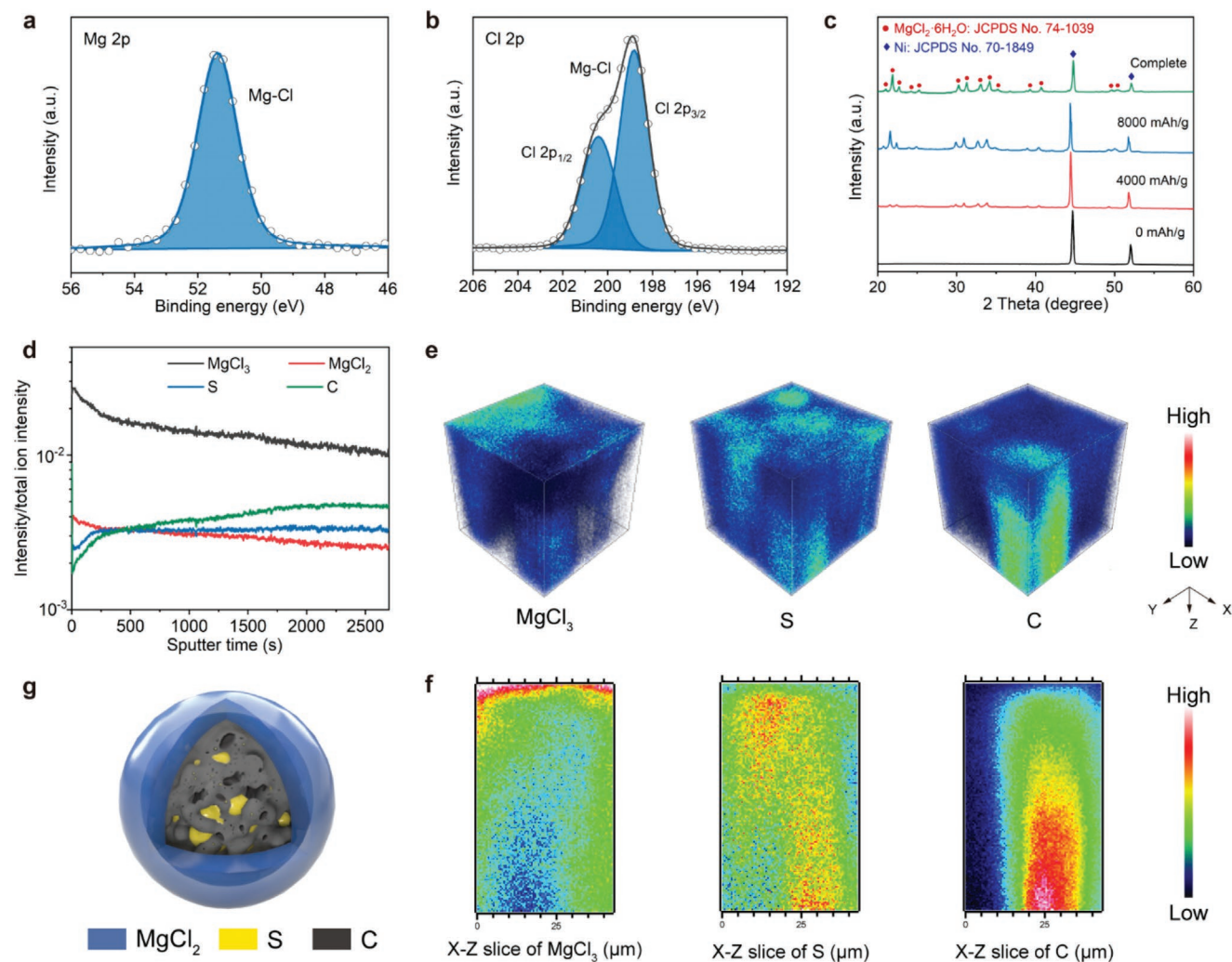
Figure 4. Distribution of the discharge products on KJ cathode. a, b) High-resolution XPS spectra for Mg 2p and Cl 2p of the KJ cathode after fully discharge, respectively. c) Ex situ XRD spectra of the KJ cathodes at different discharge depths. d) Depth profile of $MgCl_3$, $MgCl_2$, S, and C secondary ion fragments obtained by sputtering and TOF-SIMS analysis of a fully discharged KJ cathode. e) 3D distributions of $MgCl_3$, S, and C secondary ion fragments constructed from TOF-SIMS depth scan of a fully discharged KJ cathode. Analysis area is $100 \times 100 \ \mu m^2$. f) The corresponding cross-section images show the depth distribution of $MgCl_3$, S, and C secondary ion fragments. g) Schematic illustration of the distribution of $MgCl_2$, S, and C on the cathode after fully discharged.

indexed to the (001) plane of $MgCl_2$ (Figure S9c,d, Supporting Information). The diffraction spots from selected-area electron diffraction (SAED) also indicated the generation of $MgCl_2$ on the KJ cathode (inset of Figure S9c, Supporting Information). Element mapping analysis using SEM indicated the presence of C, S, Mg, and Cl on the Ni foam substrate (Figure 3e). Notably, the well-overlapped Mg and Cl mapping suggested the formation of $MgCl_2$ on the KJ cathode, consistent with the stacking cuboid and diffraction pattern of $MgCl_2$ detected in TEM. The S was mainly distributed on the surface of carbon, verified by the good overlapping of the S and C signals.

We showed the chemical composition of the main discharge products on KJ cathode via X-ray photoelectron spectroscopy (XPS) (**Figure 4**a,b). The strong Mg 2p peak at 51.2 eV confirmed the existence of Mg-Cl.[16] The pronounced Cl $2p_{3/2}$ (199.2 eV) and Cl $2p_{1/2}$ (200.4 eV) peaks were index to $MgCl_2$.[17] The crystal structural transition of the discharge products on

cathode at different discharging states was identified by the ex situ X-ray diffraction (XRD) (Figure 4c). When discharged to 4000 mAh g^{-1}, the intensity of the Ni foam began to decrease with the emerging peaks at 21.8°, 29.8°, and 34.8°, which could be assigned to $MgCl_2 \cdot 6H_2O$ (JCPDS No. 74–1039) as the $MgCl_2$ easily absorbed water in the air during measurement. As the discharging process continued, the signal intensity of $MgCl_2 \cdot 6H_2O$ increased, indicating the continuous generation of $MgCl_2$ on the cathode.

We further investigated the cathode reaction via time-of-flight secondary ion mass spectroscopy (TOF-SIMS), which reveals the evolution of secondary ion fragments as the sputtering proceeds in a negative mode. The detected $MgCl_3$, $MgCl_2$ and S secondary ion fragments are the signatures of $MgCl_2$ and S-based species during discharge (Figure S11, Supporting Information). It should be noted that the valence state of Mg is +2 for both ionized $MgCl_3$ and $MgCl_2$ fragments. The distribution

of discharged products was identified by the depth profile of selected secondary ion fragments on the cathode (Figure 4d). The decreased content of ionized $MgCl_3$ and $MgCl_2$ fragments with the increasing depth indicated that $MgCl_2$ was mainly distributed on the surface of KJ carbon. In contrast, S and C showed increasing intensities with increased sputtering depth, suggesting that S species were mainly produced in the pores of carbon. The detailed distribution of each fragment was further investigated via 3D depth profiling, which visualized that S and $MgCl_2$ were mainly distributed inside and outside the carbon core, respectively (Figure 4e). Combined with the corresponding 3D depth profile cross-section images, the results further demonstrated that S was mainly dispersed inside the carbon (Figure 4f,g). Therefore, we showed that the $MgCl_2$ products were mainly distributed on the surface of KJ carbon upon discharging, consistent with the SEM results in Figure 3a–d. Besides, $SOCl_2$ diffused into the unfilled pores of carbon to generate S, SO_2, and Cl^-. In this regard, KJ with high specific surface area and pore volume (Table S3, Supporting Information) is beneficial to $MgCl_2$ formation and $SOCl_2$ diffusion, which enables the best battery performance. In addition, the generated SO_2 can be dissolved in the $SOCl_2$-based electrolyte, preventing battery crack or electrolyte leakage originated from severe pressure changes. We are also exploring new electrolyte additives with strong adsorption or forming liquid intermediate products with SO_2 for further stabilization of the battery pressure.

The sustainability challenge of $Li/SOCl_2$ primary batteries can be readily overcome by our $Mg/SOCl_2$ chemistry, because the earth abundance of Mg (> 2%) is over 1000 times higher than Li (0.0017%)[18] Additionally, raw cost estimation suggests a much lower price of our $Mg/SOCl_2$ primary battery (≈US$4 per kilowatt hour) compared with the conventional $Li/SOCl_2$ counterpart (≈US$28 per kilowatt hour), owing to the low-cost Mg-based anode and electrolyte. We further showed that the commercial Mg-Al alloy (AZ91D) could serve as a low-cost anode (US$4.7 per kilogram) compared with metallic Li (US$170 per kilogram) and Mg (US$8.9 per kilogram) (**Figure 5**a).

It is well recognized that the recycling of end-of-life batteries represents a serious challenge,[19] particularly for $Li/SOCl_2$ batteries using highly active Li metal that can be hardly recycled or reprocessed. The use of safe and environment-friendly Mg metal provides a feasible solution to this issue. As a proof-of-concept, we recycled the carbon cathode and Mg metal anode from a "dead" $Mg/SOCl_2$ primary battery by removing the discharging products via simple and mild immersion into ethanol at air atmosphere (Figure 5b,c; Figure S12, Supporting Information). After the re-assembly with new electrolyte and separator, the battery using recycled electrodes delivered a high specific discharge capacity of 10 083 mAh g^{-1} (nearly 90% of the initial capacity) with an available discharge voltage of 1.56 V at 200 mA g^{-1}. This suggests the attractive recyclability and sustainability of these economic and environment-friendly batteries.

The safety concerns of $Li/SOCl_2$ primary batteries aroused by highly active Li metal have hindered their broad applications, evident from the battery explosion and severe injury accidents in recent years.[20] Our $Mg/SOCl_2$ primary batteries show promoted safety because the Mg metal is intrinsically less active

compared with Li metal (Figure 5d). As a proof-of-concept, we showed two $Mg/SOCl_2$ primary batteries (CR2016 coin cells) in series could power a commercial electronic watch (Figure 5e) and enable the safe operation underwater (Figure 5f). In addition, we demonstrated a high-power application using a $Mg/SOCl_2$ primary battery to power a wearable light-emitting diode (LED) array comprised of 37 in-parallel LED lamps (Figure 5g). We further used our $Mg/SOCl_2$ primary batteries to power a pair of smart glasses, an important wearable scenario in which the batteries are in close contact with the user's head and require high safety and reliability (Figure 5h). These indicate that our $Mg/SOCl_2$ primary batteries can serve as high-safety and low-cost power supplies in a variety of real-world applications.

3. Conclusion

In conclusion, we demonstrate that Mg chemistry can be a sustainable alternative for $Li/SOCl_2$ primary batteries through synergistic optimization of electrolyte solvation and electrode reaction. The presence of saturated $MgCl_2$ in the electrolyte is critical to enhance the discharge and retention performances of $Mg/SOCl_2$ primary batteries, owing to the promoted $MgCl_2$ formation along with the suppressed self-discharge corrosion. The optimized $Mg/SOCl_2$ primary battery delivers remarkable specific capacities up to ≈14000 mAh g^{-1} with a discharge plateau of ≈1.67 V. In addition, the impressive advantages of the $Mg/SOCl_2$ chemistry such as high abundance, safety, economic benefit, and recyclability make the obtained batteries promising alternatives to the state-of-the-art $Li/SOCl_2$ primary batteries. These achievements can open new avenues for development of sustainable, low-cost, recyclable, and high-performance batteries toward real-world applications.

4. Experimental Section

Preparation of the $SOCl_2$-Based Electrolytes: The electrolyte was prepared inside an Ar-filled glovebox with water and oxygen content below 2 ppm. $SOCl_2$ (99%, Aladdin), $AlCl_3$ (99%, anhydrous, Aladdin) and $MgCl_2$ (99.9%, anhydrous, Meryer) were used without further purification. The HC-A-$SOCl_2$ and A-$SOCl_2$ electrolytes were prepared by dissolving 4 M and 2 M $AlCl_3$ salt in $SOCl_2$ under stirring for 30 min, respectively. The $AlCl_3$-$MgCl_2$-$SOCl_2$ (named A-M-$SOCl_2$) electrolyte was prepared by adding 0.8 M $MgCl_2$ salt to A-$SOCl_2$, followed by stirring for 4 h or until $MgCl_2$ could no longer be dissolved. The supernatant was then collected as the electrolyte for further electrochemical characterization.

Preparation of the Cathode: The cathode slurry was prepared by mixing carbon materials (KJ, AB, or graphite) and PTFE (polytetrafluoroethylene) binder (60% aqueous dispersion) at a weight ratio of 90:10 in ethanol. The obtained mixture was sonicated for 1 h until the carbon particles were uniformly dispersed in ethanol. Ni foams with a diameter of 14 mm (1.54 cm^2) were obtained using a manual disk cutter (MTI, MSK-T-10), followed by sonication treatment in diluted hydrochloric acid (10%) for 10 min to remove the impurities on the surface. Then it was rinsed with deionized water and ethanol in sequence and dried at 80 °C before use. The prepared slurry was further dropped (100 μL each time) onto the Ni foam on an 80 °C hot plate for thorough evaporation of the solvents. The above process was repeated until the desired mass loading was achieved. KJ cathodes with the mass loadings of 1–2 and 2–3 mg cm^{-2}
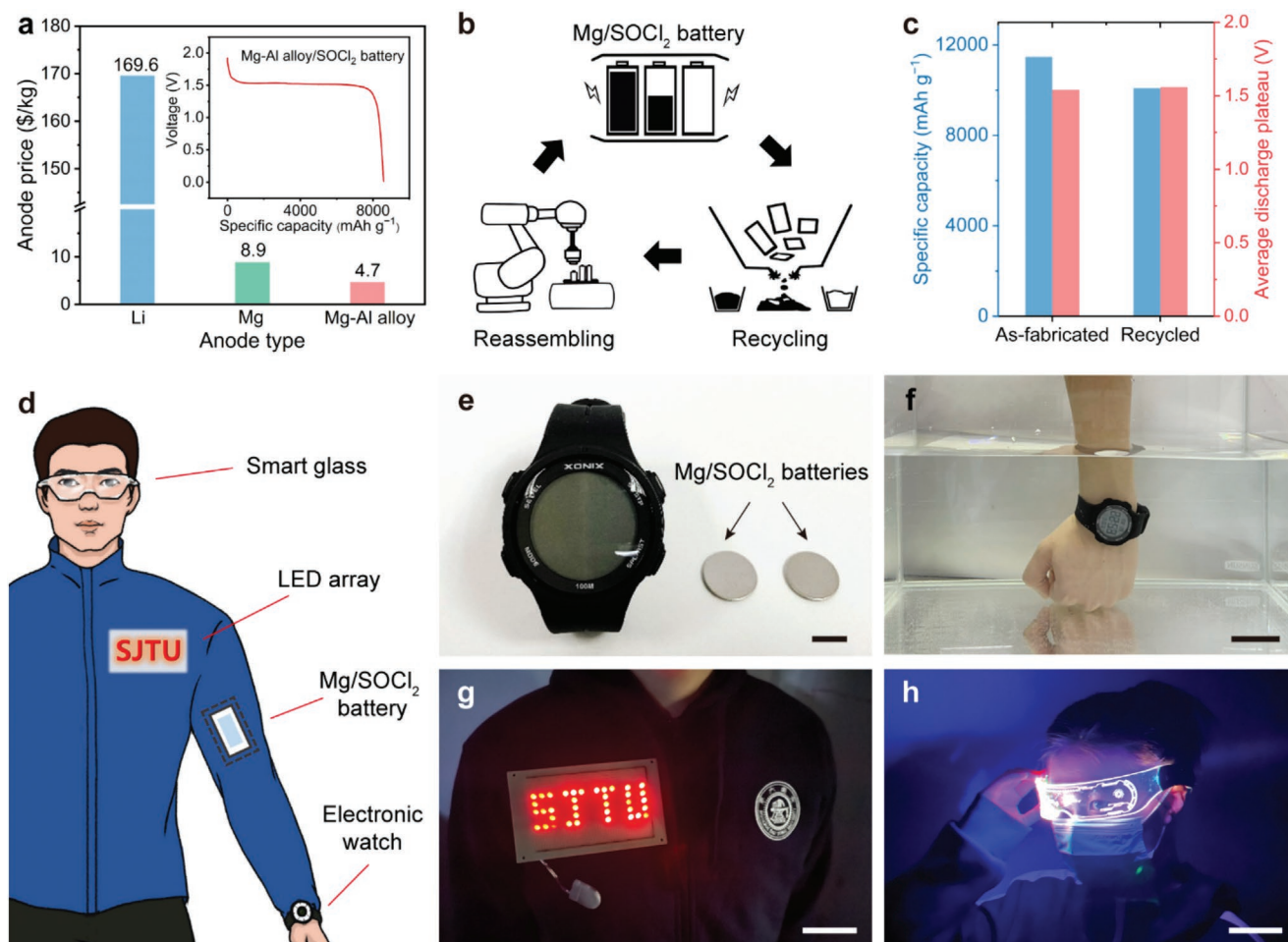
Figure 5. $Mg/SOCl_2$ primary batteries are low-cost, recyclable, and promising for wearable applications. a) Comparison of the prices of Li metal, Mg metal, and Mg-Al alloy (AZ91D). Average bulk metal prices were obtained from the Asian Metal Online Database (www.asianmetal.cn). The inset shows the discharge curve of the Mg-Al alloy/$SOCl_2$ primary battery at 100 mA g^{-1}. b) Schematic illustration of the recycling process of the $Mg/SOCl_2$ primary batteries. c) Comparison on the specific capacity and average discharge plateau of the as-fabricated and recycled battery. d) Schematic illustration of the wearable applications of $Mg/SOCl_2$ primary batteries. e, f) A commercial electronic watch and two $Mg/SOCl_2$ primary batteries working in the air and water, respectively. Scale bars in e and f, 1 cm and 5 cm, respectively. g) A wearable LED array comprised of 37 red lamps powered by a $Mg/SOCl_2$ primary battery. Scale bar in g, 5 cm. h) A pair of smart glasses powered by $Mg/SOCl_2$ batteries. Scale bar in h, 5 cm.

were prepared, followed by drying overnight at 80 °C in an oven and further pressing by a rolling pin.

Preparation of the $Mg/SOCl_2$ and $Li/SOCl_2$ Primary Batteries: All batteries were made inside an argon-filled glovebox with water and oxygen content below 2 ppm. A piece of Mg metal foil with a thickness of 100 μm was polished using an abrasive paper and cut into a rectangular shape of 1 cm × 1 cm. One layer of GF/D membrane was used as the separator. 150 μL electrolyte was used for each battery. The coin cell was encapsulated using a digital pressure controllable electric crimper (MTI, MSK-160E). A silica gel was applied to the edge of the coin cell where the two cases were sealed as an additional protective layer to prevent water and air from leaking into the battery. The preparation of $Li/SOCl_2$ primary battery involved the use of a Li metal foil as the anode, 1.8 M $LiAlCl_4$ in $SOCl_2$ as the electrolyte and AB loaded on a Ni foam as the cathode according to the commonly used composition of commercial $Li/SOCl_2$ primary batteries. The recycling of $Mg/SOCl_2$ primary battery was conducted by disassembling a fully discharged $Mg/SOCl_2$ primary battery. The KJ cathode and Mg anode were rinsed with ethanol in air atmosphere, and dried at 80 °C and room temperature, respectively. The obtained KJ and Mg electrodes were then assembled into a new battery with the incorporation of new electrolyte and separator.

Electrochemical Measurements: All the electrochemical measurements were performed at 28 °C in a thermostatic test chamber (Neware MHW-200) unless otherwise stated. The discharge performances of the batteries were obtained using a Neware battery testing system (CT-4008-5V50mA-164-U). A CHI660E electrochemical work station was used for electrochemical impedance spectroscopy (EIS) measurements. The three-electrode electrochemical impedance tests were conducted in CR2032 coin cells with a Mg metal foil as the counter and reference electrodes, and KJ loaded on a Ni foam cathode as the working electrode. The frequency ranged from 0.01 to 10^5 Hz with an amplitude at 5 mV. For wearables tested on human participants, the experiment is approved by the Institutional Review Board (IRB)/Ethical Committee and the informed consent of all participating subjects has been obtained, and the study conforms to recognized standards.

Characterizations: The Raman spectroscopy was carried out on a Renishaw inVia Micro-Raman system with an excitation laser line of 532 nm. The samples were contained in a capillary prepared in an argon-filled glove box. The XRD patterns were acquired using a Rigaku Ultima IV powder X-ray diffractometer with Cu Kα radiation. SEM was performed on a ZEISS Gemini 300 SEM operated at 15 kV. The EDS mapping was conducted with the electron beam condition of 5 kV and

**ADVANCED
SCIENCE NEWS**

www.advancedsciencenews.com

**ADVANCED
FUNCTIONAL
MATERIALS**

www.afm-journal.de

1.6 nA. TEM was performed on a JEOL JEM-2100F operated at 200 kV. For the time-of-flight secondary-ion mass spectrometry (TOF-SIMS) studies, ION-TOF TOF-SIMS 5 was used with the pressure of the analysis chamber below 1.1×10^{-9} mbar. The organic imaging with delay extraction mode with pulsed 30 keV Bi^{3+} (0.27 pA pulsed current) ion beam was applied for depth profiling analysis with 1 keV Cs^+ ion beam sputtering at the same time (69.27–82.74 nA current) and 300×300 μm^2 sputter raster. The analysis area is 100×100 μm^2. XPS spectra were collected on a Thermo Fisher Nexsa XPS Microprobe operated at 25 mA and 15 kV. All the binding energies were calibrated with the C1s peak (284.8 eV).

Supporting Information

Supporting Information is available from the Wiley Online Library or from the author.

Acknowledgements

Conflict of Interest

The authors declare no conflict of interest.

Data Availability Statement

The data that support the findings of this study are available from the corresponding author upon reasonable request.

Keywords

[1] a) M. Armand, J. M. Tarascon, *Nature* **2008**, *451*, 652; b) J. He, C. Lu, H. Jiang, F. Han, X. Shi, J. Wu, L. Wang, T. Chen, J. Wang, Y. Zhang, H. Yang, G. Zhang, X. Sun, B. Wang, P. Chen, Y. Wang, Y. Xia, H. Peng, *Nature* **2021**, *597*, 57; c) Y. Lu, J. Chen, *Nat. Rev. Chem.* **2020**, *4*, 127; d) S. Ge, Y. Leng, T. Liu, S. Longchamps Ryan, X.-G. Yang, Y. Gao, D. Wang, D. Wang, C.-Y. Wang, *Sci. Adv.* **2020**, *6*, eaay7633.

[2] J. J. Auborn, K. W. French, S. I. Lieberman, V. K. Shah, A. Heller, *J. Electrochem. Soc.* **1973**, *120*, 1613.

[3] a) K. M. Abraham, R. M. Mank, *J. Electrochem. Soc.* **1980**, *127*, 2091; b) R. Gangadharan, P. N. N. Namboodiri, K. V. Prasad, R. Viswanathan, *J. Power Sources* **1979**, *4*, 1; c) W. K. Istone, R. J. Brodd, *J. Electrochem. Soc.* **1984**, *131*, 2467; d) A. N. Dey, *Thin Solid Films* **1977**, *43*, 131; e) S.-B. Lee, S.-I. Pyun, E.-J. Lee, *Electrochim. Acta* **2001**, *47*, 855; f) F. Shen, S. Wang, Y. Gao, *Joule* **2021**, *5*, 2766.

[4] a) J.-H. Wei, *Int. J. Electrochem. Sci.* **2017**, *12*, 898; b) G. Zhu, X. Tian, H. C. Tai, Y. Y. Li, J. Li, H. Sun, P. Liang, M. Angell, C. L. Huang, C. S. Ku, W. H. Hung, S. K. Jiang, Y. Meng, H. Chen, M. C. Lin, B. J. Hwang, H. Dai, *Nature* **2021**, *596*, 525; c) M. Xia, Y. Feng, J. Wei, A. M. Rao, J. Zhou, B. Lu, *Adv. Funct. Mater.* **2022**, *32*, 2205879.

[5] a) A. N. Dey, *J. Electrochem. Soc.* **1976**, *123*, 1262; b) Z. Zhang, Kong, L. , Y. Xiong, Y. Luo, J. Li, *J. Solid State Electrochem.* **2014**, *18*, 3471; c) Y. Gao, L. Chen, M. Quan, G. Zhang, Y. Zheng, J. Zhao, *J. Electroanal. Chem.* **2018**, *808*, 8; d) K. Li, Z. Xu, Q. Liu, Z. Li, X. Wang, J. Zhang, J. Zhu, *Electrochim. Acta* **2020**, *353*, 136543; e) K. Li, J. Zhu, Q. Liu, Z. Li, J. Zhao, J. Zhang, L. Wang, Z. Xu, *J. Electrochem. Soc.* **2020**, *167*, 040506; f) Z. Xu, H. Yan, K. Yao, K. Li, J. Li, K. Jiang, Z. Li, *J. Electrochem. Soc.* **2021**, *168*, 100528.

[6] a) K. A. Klinedinst, M. J. Domeniconi, *J. Electrochem. Soc.* **1980**, *127*, 539; b) O. M. Uy, R. H. Maurer, *J. Spacecr. Rockets* **1988**, *25*, 304.

[7] a) P. Greim, A. A. Solomon, C. Breyer, *Nat. Commun.* **2020**, *11*, 4570; b) J. Ge, L. Fan, A. M. Rao, J. Zhou, B. Lu, *Nat. Sustain.* **2021**, *5*, 225; c) G. Wang, B. Kohn, U. Scheler, F. Wang, S. Oswald, M. Loffler, D. Tan, P. Zhang, J. Zhang, X. Feng, *Adv. Mater.* **2020**, *32*, 1905681. d) Y. Liang, Y. Jing, S. Gheytani, K. Y. Lee, P. Liu, A. Facchetti, Y. Yao, *Nat. Mater.* **2017**, *16*, 841.

[8] a) J. Qian, B. D. Adams, J. Zheng, W. Xu, W. A. Henderson, J. Wang, M. E. Bowden, S. Xu, J. Hu, J.-G. Zhang, *Adv. Funct. Mater.* **2016**, *26*, 7094; b) K. Liu, Y. Liu, D. Lin, A. Pei, Y. Cui, *Sci. Adv.* **2018**, *4*, eaas9820.

[9] S. Hou, X. Ji, K. Gaskell, P.-f. Wang, L. Wang, J. Xu, R. Sun, O. Borodin, C. Wang, *Science* **2021**, *374*, 172.

[10] a) A. J. Hills, N. A. Hampson, *J. Appl. Electrochem.* **1988**, *18*, 211; b) T. J. Melton, J. Joyce, J. T. Maloy, J. A. Boon, J. S. Wilkes, *J. Electrochem. Soc.* **1990**, *137*, 3865.

[11] R. E. Doe, R. Han, J. Hwang, A. J. Gmitter, I. Shterenberg, H. D. Yoo, N. Pour, D. Aurbach, *Chem. Commun.* **2014**, *50*, 243.

[12] a) B.-R. Kim, G. Jeong, A. Kim, Y. Kim, M. G. Kim, H. Kim, Y.-J. Kim, *Adv. Energy Mater.* **2016**, *6*, 1600682; b) H. Sun, G. Zhu, X. Xu, M. Liao, Y. Y. Li, M. Angell, M. Gu, Y. Zhu, W. H. Hung, J. Li, Y. Kuang, Y. Meng, M. C. Lin, H. Peng, H. Dai, *Nat. Commun.* **2019**, *10*, 3302.

[13] a) P. A. Mosier-Boss, R. D. Boss, C. J. Gabriel, S. Szpak, J. J. Smith, R. J. Nowak, *J. Chem. Soc., Faraday Trans. 1* **1989**, *85*, 11; b) R. C. Mcdonald, W. Wang, S. H. W. Hankin, *J. Phys. Chem.* **1992**, *96*, 9760; c) P. A. Mosier-Boss, S. Szpak, J. J. Smith, R. J. Nowak, *J. Electrochem. Soc.* **1989**, *136*, 1282.

[14] a) C. Li, F. Cheng, W. Ji, Z. Tao, J. Chen, *Nano Res.* **2009**, *2*, 713; b) J. Xu, Q. Yang, C. Huang, M. S. Javed, M. K. Aslam, C. Chen, *J. Appl. Electrochem.* **2017**, *47*, 767.

[15] a) B. N. Grgur, M. Gojgić, M. Petrović, *J. Power Sources* **2021**, *490*, 229549; b) M. Kong, L. Bu, W. Wang, *J. Power Sources* **2021**, *506*, 230210; c) K. V. Prasad, N. Venkatakrishnan, P. B. Mathur, *J. Power Sources* **1977**, *1*, 371.

[16] T. Gao, S. Hou, K. Huynh, F. Wang, N. Eidson, X. Fan, F. Han, C. Luo, M. Mao, X. Li, C. Wang, *ACS Appl. Mater. Interfaces* **2018**, *10*, 14767.

[17] F. Garbassi, L. Pozzi, *J. Electron Spectrosc. Relat. Phenom.* **1979**, *16*, 199.

[18] a) S. B. Son, T. Gao, S. P. Harvey, K. X. Steirer, A. Stokes, A. Norman, C. Wang, A. Cresce, K. Xu, C. Ban, *Nat. Chem.* **2018**, *10*, 532; b) H. Dong, O. Tutusaus, Y. Liang, Y. Zhang, Z. Lebens-Higgins, W. Yang, R. Mohtadi, Y. Yao, *Nat. Energy* **2020**, *5*, 1043; c) W. Ren, D. Wu, Y. NuLi, D. Zhang, Y. Yang, Y. Wang, J. Yang, J. Wang, *ACS Energy Lett.* **2021**, *6*, 3212; d) N. Wu, Z. Z. Yang, H. R. Yao, Y. X. Yin, L. Gu, Y. G. Guo, *Angew. Chem. Int. Ed.* **2015**, *54*, 5757.

[19] C. Bauer, S. Burkhardt, N. P. Dasgupta, L. A.-W. Ellingsen, L. L. Gaines, H. Hao, R. Hischier, L. Hu, Y. Huang, J. Janek, C. Liang, H. Li, J. Li, Y. Li, Y.-C. Lu, W. Luo, L. F. Nazar, E. A. Olivetti, J. F. Peters, J. L. M. Rupp, M. Weil, J. F. Whitacre, S. Xu, *Nat. Sustain.* **2022**, *5*, 176.

[20] E. Hennesø, F. H. Hedlund, *J. Fail. Anal. Prev.* **2015**, *15*, 600.